ADVANCED FUNCTIONAL MATERIALS
www.afm-journal.de

Materials Views
www.MaterialsViews.com

Co_3O_4 Nanoparticles as Robust Water Oxidation Catalysts Towards Remarkably Enhanced Photostability of a Ta_3N_5 Photoanode

Maijia Liao, Jianyong Feng, Wenjun Luo, Zhiqiang Wang, Jiyuan Zhang, Zhaosheng Li, Tao Yu, and Zhigang Zou*

Despite the fact that Ta_3N_5 absorbs a major fraction of the visible spectrum, the rapid decrease of photocurrent encountered in water photoelectrolysis over time remains a serious hurdle for the practical application of Ta_3N_5 photoelectrodes. Here, by employing a Co_3O_4 nanoparticle water oxidation catalyst (WOC) as well as an alkaline electrolyte, the photostability of Ta_3N_5 electrode is significantly improved. Co_3O_4/Ta_3N_5 photoanode exhibits the best durability against photocorrosion to date, when compared with $Co(OH)_x/Ta_3N_5$ and IrO_2/Ta_3N_5 photoanodes. Specifically, about 75% of the initial stable photocurrent remains after 2 h irradiation at 1.2 V vs. RHE (reversible hydrogen electrode). Meanwhile, a photocurrent density of 3.1 mA cm^{-2} has been achieved on Co_3O_4/Ta_3N_5 photoanode at 1.2 V vs. RHE with backside illumination under 1 sun AM 1.5 G simulated sunlight. The reason for the relatively high stability is discussed on the basis of electron microscopic observations and photoelectrochemical measurements, and the surface nitrogen content is monitored by X-ray photoelectron spectroscopic analysis.

1. Introduction

Efficient solar energy conversion and storage technologies offer desirable approaches to ameliorate stringent global energy demands and environmental sustainability[1] Photoelectrochemical (PEC) water splitting is a potential way to capture and store the earth's abundant solar energy influx.[2] Metal oxides, on account of their good photostability and relatively high solar energy conversion efficiency, are extensively studied as photoelectrodes for PEC conversion of solar energy into chemical fuels.[3–5] However, due to the deeply located energy potential of O 2p orbitals, which comprise the whole or majority of the valance band maximum, visible-light-responsive metal oxide photoelectrodes often possess insufficient reduction potential, and as a result an externally applied bias is inevitable. Meanwhile, considerable efforts have been focusing on non-oxide semiconductors with smaller band gaps and appropriate energy levels for PEC H_2 production.[6,7] However, the biggest challenge presently confronted for the practical application of these non-oxide semiconductors is how to improve chemical- and photo-stability in aqueous environment.[8,9] Among these non-oxide semiconductors, (oxy)nitrides containing Ta^{5+} or Ti^{4+}, such as TaON, Ta_3N_5 and $LaTiO_2N$, emerge as promising candidates for PEC overall water splitting, because these (oxy)nitrides materials are able to reduce and oxidize water in the presence of appropriate sacrificial reagents under visible-light irradiation.[10–13] The stable activities for photocatalytic H_2 or O_2 evolution suggest their great potential as highly efficient and long durable photoelectrodes working under visible-light irradiation without auxiliary voltage. Recently, Ta_3N_5 photoelectrode has attracted intensive interest, because its maximum possible solar-to-hydrogen efficiency is as high as 15.9% under AM 1.5 G irradiation.[14]

However, owing to the self-oxidative decomposition of Ta_3N_5 in which nitrogen anions are oxidized to N_2 by photogenerated holes, the photocurrent of bare Ta_3N_5 photoanode becomes negligibly low within few minutes.[14b] So far, the reported half-value period of the photocurrent for IrO_2 loaded Ta_3N_5 has been estimated to be less than 10 minutes, indicating that the stability remains miserably poor for water splitting.[15] Steady photocurrent on Ta_3N_5 photoelectrode was only obtained in aqueous $Fe(CN)_6^{3-}/Fe(CN)_6^{4-}$ solution, which is attributable to the higher activity for $Fe(CN)_6^{4-}$ oxidation compared to water oxidation.[16] The rapid decrease of photocurrent encountered in the water photoelectrolysis, even after IrO_2 modification, seriously prohibits the practical application of Ta_3N_5 photoelectrode. Nevertheless, even for the generally regarded stable metal oxides photoelectrodes, such as hematite and tungsten trioxide, they exhibit good photochemical stabilities only in basic and acidic aqueous solution, respectively.[3,4] Our group also found that the selection of electrolyte is pivotal to the stability of

M. J. Liao, J. Y. Feng, Dr. W. J. Luo, Z. Q. Wang, J. Y. Zhang, Prof. Z. S. Li, Prof. T. Yu, Prof. Z. G. Zou
Ecomaterials and Renewable Energy Research Center
National Laboratory of Solid State Microstructures
Nanjing University
Nanjing 210093, China
E-mail: zsli@nju.edu.cn
J. Y. Feng, Prof. Z. S. Li
College of Engineering and Applied Science
Nanjing University
Nanjing 210093, China

DOI: 10.1002/adfm.201102966

InGaN photoanode.[17] These facts imply that there is a means to stabilize the Ta_3N_5 photoelectrode by applying an appropriate electrolyte instead of the most commonly used Na_2SO_4.

At the same time, the presently used precious metal oxide IrO_2 acts as a dissatisfactory WOC, due to its instability nature and poor distribution on the Ta_3N_5 surface.[15,5e] Hence, concomitant with the consideration for the cost of WOCs, there comes more strict requirements on the efficiency and stability of WOCs loaded on Ta_3N_5 photoanode, for the reason that WOCs bear the responsibility of efficient promotion of O_2 evolution and long durability against chemical- and photo-corrosion in the selected electrolyte environment. Cobalt oxides, harboring two conspicuous merits of high activity for O_2 evolution and low cost, emerge as robust WOCs. Crystalline Co_3O_4 films have been proved to be catalytically efficient and stable in water electrolysis reaction in an alkaline solution.[18,19] Current density as high as 10 mA/cm^2 has been achieved at overpotential of 328 mV on nanoparticulated Co_3O_4 anode with a loading amount of 1 mg/cm^2.[20]

In this study, Ta_3N_5 photoelectrode is expected to offer improved stability by using crystalline Co_3O_4 nanoparticles WOC, which largely helps to release photogenerated holes accumulated on the Ta_3N_5 surface. The removing of protons participates in water oxidation reaction, while the proton accepting ability is different for NaOH and Na_2SO_4 electrolytes. The effect of NaOH and Na_2SO_4 electrolyte on PEC performance of Ta_3N_5 photoelectrode is also investigated.

2. Results and Discussion

2.1. Effect of the Electrolyte on PEC Performance of Bare Ta_3N_5 Photoanodes

In powder suspension system, not only the photocatalytic activity for O_2 evolution but also the durability of Ta_3N_5 is terribly discouraging under acidic condition. Only with the assistance of La_2O_3, which behaves as a pH buffer, can Ta_3N_5 achieve steady and prompt O_2 production.[10,11] Alkaline condition seems to be favorable for promoting O_2 evolution and inhibiting N_2 generation. These facts indicate that basic environment may benefit the long durability of Ta_3N_5 photoanodes. Exploration experiments were conducted in most commonly used Na_2SO_4 (0.5 M, pH = 6.5) and NaOH (1 M, pH = 13.6), in order to reveal the differences of PEC performances initiated by the application of different electrolytes. **Figure 1** shows the photocurrent density-potential curves measured in NaOH and Na_2SO_4 electrolytes under visible-light irradiation ($\lambda \geq 420$ nm). The obtained results clearly reveal the sharp differences in photocurrent collected in NaOH and Na_2SO_4. Higher photocurrent values throughout the measured potential range are achieved in NaOH compared to Na_2SO_4 at the same potentials, and at higher potentials the upgrade is more evident. This result is in accordance with the powder suspension system that alkaline condition is favorable for oxidation of water by Ta_3N_5.[10,11]

2.2. Identification of Loaded Co Species

Co species colloids were prepared by addition of NaOH into an aqueous solution containing Co^{2+} ions, and deposited as WOCs onto Ta_3N_5 photoanode by an impregnation method. To identify the Co species WOCs, the colloids were washed by water and deposited onto glass slides for characterization. X-ray diffraction (XRD) analysis reveals that Co colloids film calcined at 573 K for 10 minutes may be roughly assigned as Co_3O_4, and Co colloids film prepared at room temperature contain $Co(OH)_2$ and other unknown impurity (shown in Figure S2, Supporting Information). The chemical states of Co atoms loaded onto the Ta_3N_5 photoanodes were detected by X-ray photoelectron spectroscopic analysis (XPS). Figure S3 (Supporting Information) shows the Co 2p XPS spectra of the Co species loaded photoanodes prepared at room temperature and calcined at 573 K for 10 minutes. The differences between the composite photoanodes prepared at room temperature and calcined at 573 K for 10 minutes are indistinguishable, thus failing to distinguish them from each other. To investigate them further, a Raman study was carried out on these Co species films deposited on glass slides. For an unambiguous assignment of the Raman peaks, reference sample was prepared by pasting commercial Co_3O_4 slurry onto a glass slide. The similar Raman peaks for commercial Co_3O_4 and Co species film prepared at 573 K can be ascribed to the formation of Co_3O_4 upon calcination (shown in Figure S4, Supporting Information).[21] Co species film prepared at room temperature poses similar chemical states of Co atoms with Co_3O_4, however, it exhibits Raman peaks that are difficult to identify (shown in Figure S4, Supporting Information). Combining with the XRD analysis, Co species WOC prepared at room temperature is denoted as $Co(OH)_x$ hereafter.

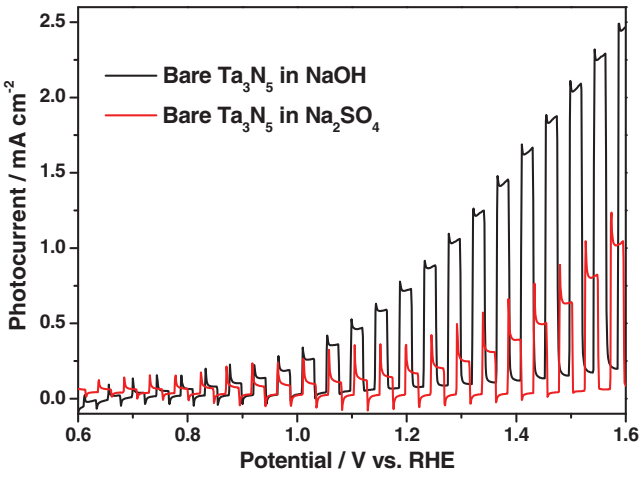

Figure 1. Photocurrent densities of bare Ta_3N_5 photoanodes in 1 M NaOH (black) and 0.5 M Na_2SO_4 (red) under visible-light irradiation ($\lambda \geq 420$ nm). Unless specifically noted, all photocurrent-voltage data are collected at the scan rate of 30 mV/s.

2.3. PEC Performance of Modified Ta_3N_5 Photoanodes (Co_3O_4/Ta_3N_5 and $Co(OH)_x/Ta_3N_5$ Composite Photoanodes)

Proper surface modification with WOCs will greatly improve the PEC performance of Ta_3N_5 electrode.[15] **Figure 2** plots the photocurrent densities versus voltage for bare Ta_3N_5 with and without short heat treatment compared to Co_3O_4/Ta_3N_5 and

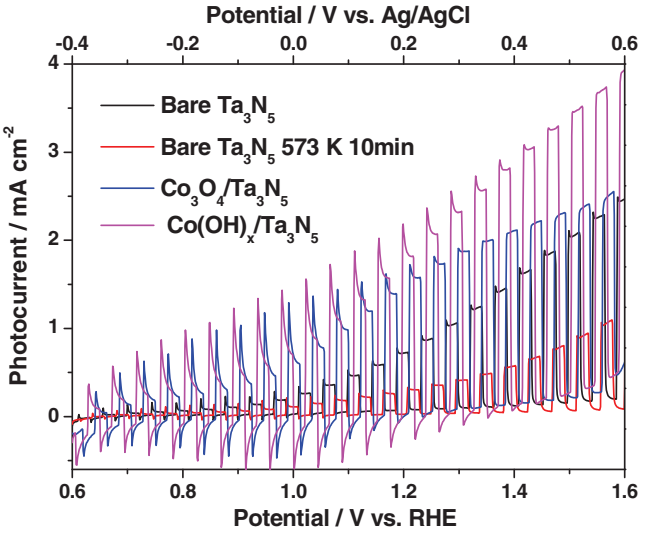

Figure 2. Photocurrent densities under visible light irradiation ($\lambda \geq$ 420 nm) of $Co(OH)_x/Ta_3N_5$ photoanode prepared by impregnation of $Co(OH)_x$ colloids onto Ta_3N_5 (mauve), Co_3O_4/Ta_3N_5 photoanode prepared by calcining $Co(OH)_x/Ta_3N_5$ at 573 K for 10 minutes in air (blue), bare Ta_3N_5 without any treatment (black), and bare Ta_3N_5 electrode subjected to calcination at 573 K for 10 minutes (red). The electrolyte is 1 M NaOH (pH = 13.6).

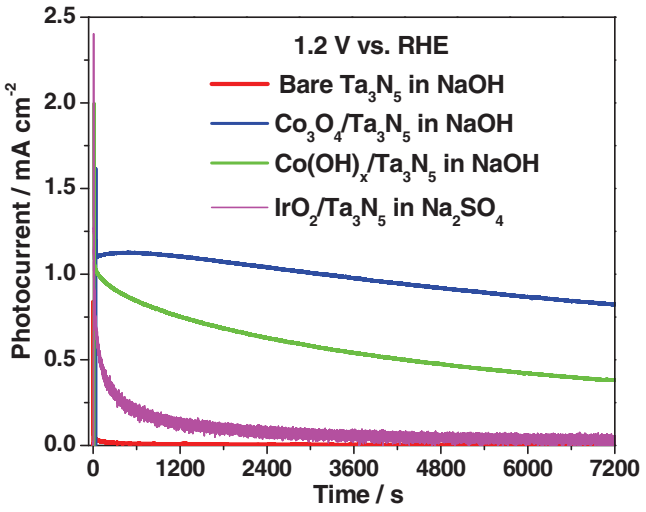

Figure 3. Photocurrent decay curves measured at 1.2 V vs. RHE under visible light irradiation ($\lambda \geq$ 420 nm) for Co_3O_4/Ta_3N_5 (in blue), $Co(OH)_x/Ta_3N_5$ (in green), bare Ta_3N_5 (red) photoelectrodes in 1 M NaOH (pH = 13.6) solution and IrO_2/Ta_3N_5 (mauve) in 0.5 M Na_2SO_4 solution (pH = 6.5). The $Co(OH)_x/Ta_3N_5$ photoanode was prepared by impregnation of $Co(OH)_x$ colloids onto Ta_3N_5, the IrO_2/Ta_3N_5 photoanode was prepared by impregnation of IrO_2 colloids onto Ta_3N_5, and Co_3O_4/Ta_3N_5 photoanode was prepared by calcining $Co(OH)_x/Ta_3N_5$ at 573 K for 10 minutes in air.

$Co(OH)_x/Ta_3N_5$ photoanodes under visible-light irradiation ($\lambda \geq$ 420 nm). Bare Ta_3N_5 electrode, as shown in Figure 2, is unable to withstand heat treatment at high temperature due to the bad thermal stability of Ta_3N_5 material itself, which results in a sharp decrease in photocurrent. As we expect, Co_3O_4 and $Co(OH)_x$ modified Ta_3N_5 electrodes show better performances relative to bare Ta_3N_5 electrode in the full tested potential range. The promotional effect is more pronounced in the lower potential region than in the higher potential region. Specifically, the photocurrent at higher bias is lower for Co_3O_4 loaded Ta_3N_5 photoanode as compared to $Co(OH)_x$ loaded Ta_3N_5 photoanode, and this slight decline for Co_3O_4 loaded Ta_3N_5 photoanode should result from heat treatment. It is interesting to note that $Co(OH)_x$ modified Ta_3N_5 photoanode behaves better thermal stability with respect to bare Ta_3N_5 photoanode. It seems credible $Co(OH)_x$ may serve as an efficient protection layer for Ta_3N_5 electrode during the short firing process, which also suggests the uniform and sufficient coverage of Ta_3N_5 surface by $Co(OH)_x$.

As mentioned above, the serious obstacle that hinders the practical application of (oxy)nitrides photoelectrodes is the poor photocurrent stability during water splitting reaction.[22] The major aim of this study is to improve the photostability of Ta_3N_5 photoelectrode. However, solely basic environment provided by NaOH electrolyte seems far from satisfying. As shown in **Figure 3**, a large initial spike in current density appears for bare Ta_3N_5 photoelectrode followed by an exponential decrease, and the steady state photocurrent is negligibly low in few seconds. The large initial spike in photocurrent upon illumination for bare Ta_3N_5 may be related with the capacitance component at the solid-liquid interface, and the rapid decrease in the photocurrent is associated with the bad photostability of Ta_3N_5.[23] Actually, slow kinetics for water oxidation usually results in holes accumulation at the surface, and subsequent surface oxidative decomposition of Ta_3N_5 occurs. Consequently, WOCs loaded onto the Ta_3N_5 surface may prompt the O_2 evolution and hinder self-oxidative decomposition of Ta_3N_5, which is favorable for the photostability of Ta_3N_5 photoelectrode. As can be seen, the photocurrent decay curves for $Co(OH)_x/Ta_3N_5$ and Co_3O_4/Ta_3N_5 photoanodes show substantial enhancement in photostability. Similar spikes are also found on both $Co(OH)_x/Ta_3N_5$ and Co_3O_4/Ta_3N_5 electrodes, and some of the initial spikes in the current densities may be attributed to cobalt oxidation, which is an essential step in the water oxidation mechanism.[24] Sustaining decrease in the photocurrent is observed on $Co(OH)_x/Ta_3N_5$ photoanode during 2 h visible-light irradiation under positive bias in alkaline solution, and this decline trend is similar with that of IrO_2 modified Ta_3N_5 photoanode.[15] An unexpected phenomenological observation on Co_3O_4/Ta_3N_5 photoanode is that a small gradual increase to steady state is followed by asymptotic decrease in photocurrent, while only exponential decay to a lower current densities are obtained on both $Co(OH)_x/Ta_3N_5$ and bare Ta_3N_5 photoanodes. Noticeably, after visible-light irradiation for 2 h, about 75% of the initial stable state photocurrent is maintained for Co_3O_4/Ta_3N_5 photoanode, while for $Co(OH)_x/Ta_3N_5$ photoanode this value is only less than 38%. Dark for a time interval of several seconds and illuminating the photoanodes again cannot recover the photocurrent of both $Co(OH)_x/Ta_3N_5$ and Co_3O_4/Ta_3N_5 photoanodes, suggesting that the photocurrent decay is not derived from the kinetic bottleneck in the O_2 evolution reaction and deleterious reactions must occur irreversibly during the PEC measurement. For comparison, we have also tested the photostability of IrO_2/Ta_3N_5 photoanode, which shows inferior photostability to both $Co(OH)_x/Ta_3N_5$ and Co_3O_4/Ta_3N_5 photoanodes.

During the course of stability measurement, bubbles were observed on the surface of photoanodes, indicating the formation of O_2 upon light irradiation. As a result, the decrease in photocurrent of $Co(OH)_x/Ta_3N_5$ photoanodes might be partially attributed to O_2 evolution induced detachment of $Co(OH)_x$ WOC. Compared with $Co(OH)_x/Ta_3N_5$, Co_3O_4/Ta_3N_5 photoanode exhibits better photocurrent stability because Co_3O_4 WOC may firmly anchored onto Ta_3N_5 surface with the assistance of heat treatment. The integration of photocurrent decay curve of the Co_3O_4/Ta_3N_5 photoanode shows that 7.1 C of electrons has passed through the circuit during 2 h measurement, corresponding to 73.6 μmol of electrons, while the estimated amount of corresponding Ta_3N_5 is ca. 0.6 μmol and the amount of loaded Co_3O_4 is 0.02 μmol (estimated from the energy dispersive X-ray results, EDX). The turnover number in this reaction is calculated to be 123 on the basis of Ta_3N_5, indicating that the majority of photocurrent on Co_3O_4/Ta_3N_5 photoanode is associated with water oxidation, not merely caused by the self-oxidative decomposition of the Ta_3N_5 itself.

2.4. SEM and TEM Investigation of Modified Ta_3N_5 Photoanodes

It is urgent to depict the distribution of $Co(OH)_x$ and Co_3O_4 WOCs on the Ta_3N_5 surface, for protecting effect provided by $Co(OH)_x$ during heat treatment as well as greatly improved PEC performance including photocurrent and photostability may largely depend on the existing status of WOCs.[15] **Figure 4** shows scanning electron microscopic (SEM) images of $Co(OH)_x/Ta_3N_5$ and Co_3O_4/Ta_3N_5 photoanodes. Inset in Figure 4a indicates that bare Ta_3N_5 particles are irregular in the size range of several hundred nanometers and their porous surfaces are formed during nitridation.[10] With respect to the bare Ta_3N_5, $Co(OH)_x$ loaded Ta_3N_5 electrode reveals slightly obscurer surface, which is ascribed to the coverage of $Co(OH)_x$. Meanwhile, fairly uniform distribution of $Co(OH)_x$ can be observed on a large scale, which may contribute to the protecting effect during thermal treatment and improved PEC performance of $Co(OH)_x$ loaded Ta_3N_5 electrode. In addition, we perform EDX analysis on a large area of the $Co(OH)_x$ loaded Ta_3N_5 film, and the element mapping of cobalt yields similar result with SEM observation, implying uniform $Co(OH)_x$ coverage on the large scales of Ta_3N_5 electrode (shown in Figure 4c). Figure 4b reveals that distinct Co_3O_4 nanoparticles with diameter of about 10 nm are dottedly distributed on the Ta_3N_5 surface. The relatively larger Co_3O_4 nanoparticles compared to $Co(OH)_x$ is mainly aroused by thermal treatment, and thermal treatment also leads to more sparse distribution of Co_3O_4 on the Ta_3N_5 surface, as can be identified by the SEM observations and element mapping of cobalt (see Figure 4b,d). Nevertheless, in the case of Co_3O_4/Ta_3N_5 photoanode, the distribution of Co_3O_4 on the Ta_3N_5 surface is still uniform as displayed by the element mapping of cobalt. Overall, both $Co(OH)_x/Ta_3N_5$ and Co_3O_4/Ta_3N_5 photoanodes show uniform distribution of the WOCs, even though the latter suffers short firing treatment. Therefore, the well distribution of WOCs may contribute greatly to the improved PEC performance of the photoelectrodes.

However, from the SEM and EDX analysis we can only explain why the photocurrent and photostability of composite photoelectrodes are improved, and the reasons for different photostability exhibited on $Co(OH)_x/Ta_3N_5$ and Co_3O_4/Ta_3N_5 photoelectrodes still should be digged out. Transmission electron microscopic (TEM) measurements were conducted to uncover the underlying discrepance between $Co(OH)_x/Ta_3N_5$ and Co_3O_4/Ta_3N_5 photoelectrodes. The $Co(OH)_x/Ta_3N_5$ and Co_3O_4/Ta_3N_5 particles were peeled from the corresponding photoelectrodes for TEM observation. As can be clearly seen in **Figure 5**a, floccules cover the porous Ta_3N_5 particles sufficiently as indicated by the black arrows, and even the surfaces of inner pores are occupied by these floccules (denoted by a white arrow and a circle). The amorphous nature of these floccules is determined by high-resolution TEM (HRTEM) characterization collected from the interfacial region (indicated by a white square). The lattice spacing of 0.28 nm can be readily assigned to (0 2 3) crystal plane of Ta_3N_5 (JCPDS 79-1533), and Ta_3N_5 particles are bonded with these floccules. The amorphous floccules are finally identified as $Co(OH)_x$ instead of products associated with postnecking treatment by $TaCl_5$, for the apparent shape of TaON or N-doped Ta_2O_5 bridges deriving from $TaCl_5$ treatment is

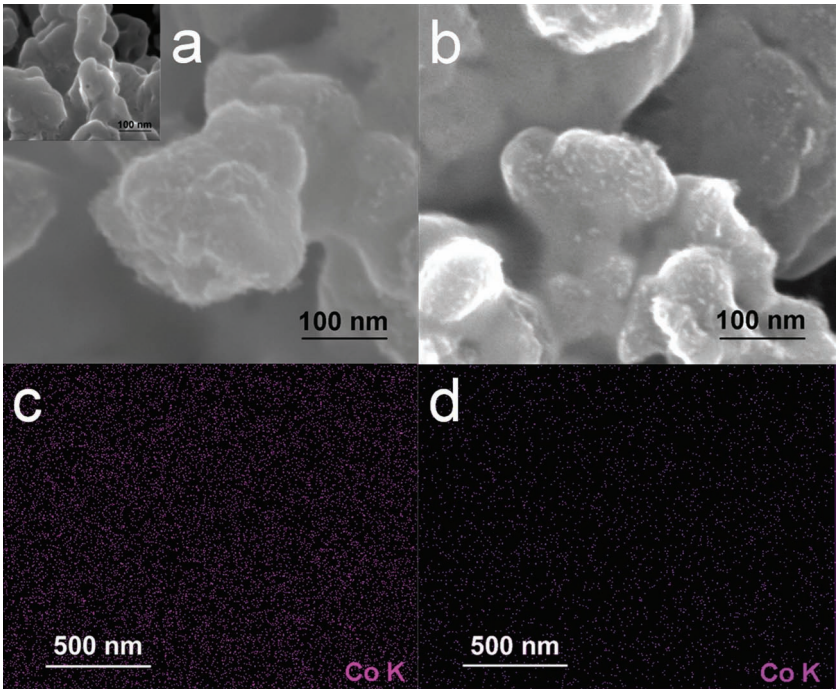

Figure 4. SEM images showing highly magnified views of a) $Co(OH)_x/Ta_3N_5$ and b) Co_3O_4/Ta_3N_5 photoanodes. Maps of the Co (K) signal intensity of c) $Co(OH)_x/Ta_3N_5$ and d) Co_3O_4/Ta_3N_5 photoanodes on the large scale. Inset in (a) shows the high-magnification SEM image of the bare Ta_3N_5 photoanode.

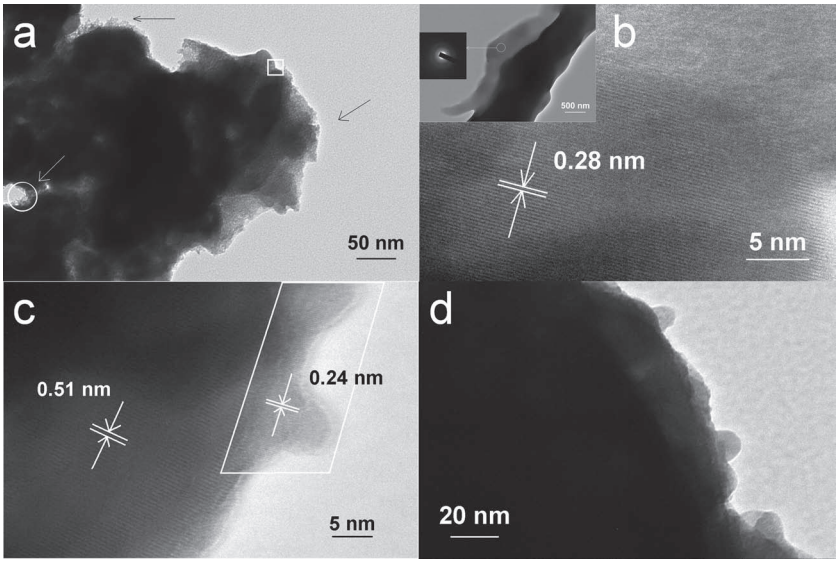

Figure 5. a) Low-magnification and b) high-resolution TEM images of Ta_3N_5 particles peeled from the $Co(OH)_x/Ta_3N_5$ photoanode. c) High-resolution and d) low-magnification TEM images of Ta_3N_5 particles peeled from Co_3O_4/Ta_3N_5 photoanode. Inset in (b) shows low magnification TEM image and selected area electron diffraction (SAED) pattern of a Ta_3N_5 particle peeled from the Ta_3N_5 photoanode after postnecking treatment for reference.

quite different from these floccules. Additionally, TaON or N-doped Ta_2O_5 bridges behave as a semi-transparent but monolithic object while $Co(OH)_x$ nanoparticles are more discrete (see inset in Figure 5b). Upon short calcination, amorphous $Co(OH)_x$ floccules are converted into Co_3O_4 nanoparticles, because interplanar distance of 0.24 nm can be indexed as (3 1 1) crystal plane of Co_3O_4 (JCPDS 42-1467). The result is also in good accordance with Raman analysis. The Co_3O_4 nanoparticles are in the size range of several nanometers, indicating that $Co(OH)_x$ floccules tend to aggregate into larger particles upon heat treatment. Panel (d) in Figure 5 depicts the distribution of Co_3O_4 WOC on Ta_3N_5 surface, as the hemispherical particles with diameter of ca. 10 nm can be assigned to Co_3O_4. The distribution of Co_3O_4 WOC is inferior to that of $Co(OH)_x$, which is consistent with SEM and EDX analysis, and the slight aggregation of Co_3O_4 nanoparticles WOC is aroused by thermal treatment.

Panel (c) in Figure 5 also shows the (0 2 0) crystal plane of Ta_3N_5 with lattice spacing of 0.51 nm. The most noticeable changes upon calcination are the formation of large-scale interfacial contacts between the Ta_3N_5 matrix and Co_3O_4 WOC, as pointed out by a white parallelogram. The nanojunctions between Ta_3N_5 matrix and Co_3O_4 nanoparticles WOC are so compact that they may ensure efficient transfer of photogenerated holes across the interfaces. Meanwhile, the compact interfaces signify the good mechanical strength of Co_3O_4 nanoparticles WOC anchoring onto Ta_3N_5 surface. Besides, the interfacial electronic structure might also contribute to the superior performance of Co_3O_4/Ta_3N_5 photoelectrode.[5a] Therefore, heat treatment is favorable for the formation of large scale and compact nano-junctions although it can also lead to the unfavorable oxidation of Ta_3N_5. Upon heat treatment the photostability of Co_3O_4/Ta_3N_5 electrode is improved, which is at the expense of the decreased photocurrent. Through this unique short firing process, we achieve the optimal PEC performance balanced between the photostability and activity.

2.5. Effect of the Electrolyte on the PEC Performances of Modified Ta_3N_5 Photoanodes

Up to now, pronounced enhancement in photostability of Co_3O_4/Ta_3N_5 photoelectrode can be explained at least partly by the uniformly distributed and compact nanojunctions formed between Co_3O_4 nanoparticles and Ta_3N_5 matrix. It is required to understand the role of NaOH electrolyte in improving the PEC performance of Co_3O_4/Ta_3N_5 photoelectrode. Then the photocurrent of Co_3O_4/Ta_3N_5 photoanode was tested in 0.5 M Na_2SO_4 in order to exclude the effect of basic condition. As shown in inset of **Figure 6**, Co_3O_4/Ta_3N_5 performs much better in the NaOH electrolyte than in Na_2SO_4 electrolyte, which is analogous with bare Ta_3N_5 (Figure 1) and $Co(OH)_x/Ta_3N_5$ photoelectrodes (see Figure S5, Supporting Information). These data clearly reveal the superiority of alkaline solution as the supporting electrolyte for better PEC performances on Ta_3N_5 photoelectrodes.

As water oxidation reaction involves the removing of protons, it is conceivable that slow water oxidation kinetics may be not only induced by inappropriate modification of WOCs, but also closely interrelated with the poor proton-accepting capability of the supporting electrolyte.[25] In Na_2SO_4 electrolyte, protons elimination depends on their diffusion into bulk solution

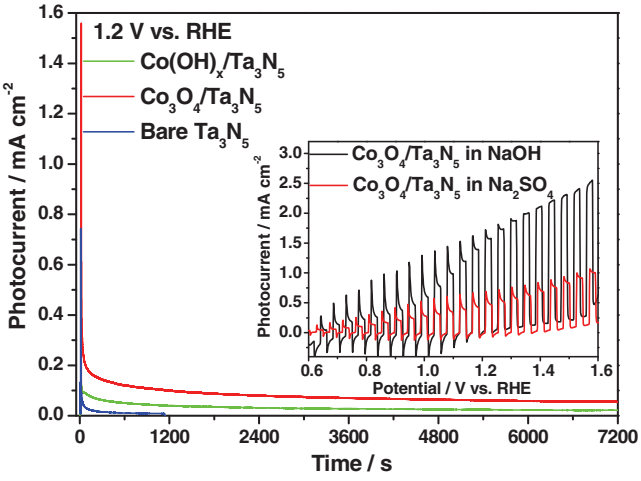

Figure 6. Photocurrent decay curves measured at 1.2 V vs. RHE under visible light irradiation ($\lambda \geq 420$ nm) for Co_3O_4/Ta_3N_5 (red), $Co(OH)_x/Ta_3N_5$ (green) and bare Ta_3N_5 (blue) photoelectrode in 0.5 M Na_2SO_4 (pH = 6.5) solution. Inset shows photocurrent densities of Co_3O_4/Ta_3N_5 composite photoanodes in 1 M NaOH (black) and 0.5 M Na_2SO_4 (red) under visible light irradiation ($\lambda \geq 420$ nm).

and the diffusion process is slow, therefore, holes accumulation and slow water oxidation kinetics are expected. For metal oxide photoelectrodes, holes accumulation usually results in recombination of electrons and holes, which is unfavorable for water splitting but can be effectively circumvented by large applied potentials.[3c] As for Ta_3N_5 photoelectrodes, when the consumption of holes by water oxidation is inefficient, holes accumulation will be alternatively alleviated through self-oxidative decomposition of Ta_3N_5. Avoiding the holes accumulation and accelerating the water oxidation kinetics are pivotal to improve the PEC property of Ta_3N_5 photoelectrodes, especially their photostability.

From the above analysis, none of the Co_3O_4/Ta_3N_5, $Co(OH)_x/Ta_3N_5$ and bare Ta_3N_5 photoanodes can achieve satisfying photostability when Na_2SO_4 is applied. As we anticipated, the photocurrent decay curves collected in Figure 6 show sharp decrease following the initial high spikes within few seconds. This result upholds our hypothesis that poor proton-accepting electrolyte will increase the O_2 evolution kinetic barrier and do harm to the photostability of Ta_3N_5. Accordingly, comparing with Na_2SO_4, the mechanism of NaOH electrolyte in promoting the PEC performance of Co_3O_4/Ta_3N_5 photoelectrode can be explained by its better proton-accepting ability.[3c]

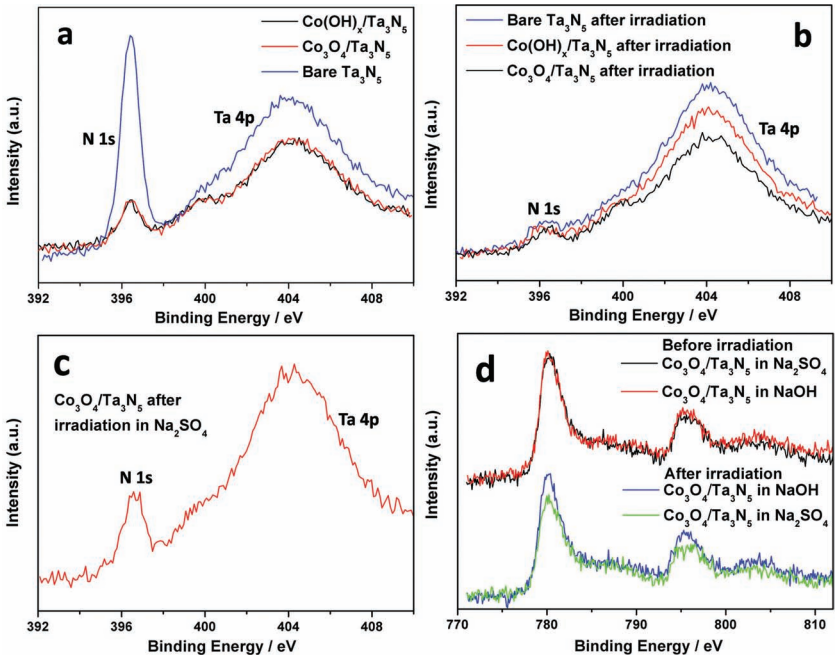

Figure 7. XPS spectra of a) N 1s for bare Ta_3N_5, $Co(OH)_x/Ta_3N_5$ and Co_3O_4/Ta_3N_5 photoelectrodes before photostability measurement; b) N 1s for bare Ta_3N_5, $Co(OH)_x/Ta_3N_5$ and Co_3O_4/Ta_3N_5 photoelectrodes under visible light irradiation for 2 h at 1.2 V vs. RHE in 1 M NaOH (pH = 13.6); c) N 1s for Co_3O_4/Ta_3N_5 photoelectrode under visible light irradiation for 2 h at 1.2 V vs. RHE in 0.5 M Na_2SO_4 (pH = 6.5); and d) Co 2p for Co_3O_4/Ta_3N_5 photoelectrodes before and after photostability measurement in 1 M NaOH and 0.5 M Na_2SO_4, photostability measurements were conducted at 1.2 V vs. RHE for 2 h under visible light irradiation ($\lambda \geq 420$ nm).

The bad photostability of Co_3O_4/Ta_3N_5 photoanode in Na_2SO_4 may come from the poor chemical stability of Co_3O_4 and/or the kinetic bottleneck of water oxidation. The former is due to the acidic neighbouring environment after O_2 production, and the latter is associated with low protons removing rate by Na_2SO_4 electrolyte. Besides WOCs, slow kinetics of water oxidation may also derive from electrolytes. We have compared the photocurrents of bare Ta_3N_5 electrodes in Na_2SO_4 and NaOH solution, for O_2 evolution kinetic barrier can only be ascribed to the proton removing rates by the electrolytes for bare Ta_3N_5 electrodes. The PEC results (shown in Figure 1) justify that a poor proton-accepting electrolyte indeed contributes to O_2 evolution kinetic barrier, and explain why the durability of Ta_3N_5 is terribly discouraging under acidic condition in powder suspension system.[10,11] This finding sheds light on the importance of facilitating the kinetics of water oxidation, which is associated with both WOCs and the electrolyte, only through parallel optimization of both WOCs and the electrolyte can we achieve efficient and steady O_2 evolution.

2.6. XPS Analysis of Ta_3N_5 Photoanodes Before and After Light Irradiation

As surface nitrogen contents are important parameters for evaluating the PEC properties of Ta_3N_5 photoelectrodes, surface nitrogen contents under different conditions were monitored by XPS analysis on these composite and bare Ta_3N_5 photoanodes. Panel (a) in **Figure 7** clearly illustrates that after loading of $Co(OH)_x$ and Co_3O_4 WOCs on Ta_3N_5 the intensity of N 1s peaks shrink largely compared to bare Ta_3N_5 film, which is due to the shielding effect of $Co(OH)_x$ and Co_3O_4 coverage on the Ta_3N_5 surface. After photostability measurement in 1 M NaOH, the N 1s peak of bare Ta_3N_5 becomes merely distinguishable while before current-time measurement N 1s peak is intense, and this sharp decay is due to the serious surface oxidation of Ta_3N_5 (shown in Figure 7b).[23] In contrast, surface nitrogen losses of Ta_3N_5 after $Co(OH)_x$ and Co_3O_4 modification are greatly suppressed although Co_3O_4/Ta_3N_5 and $Co(OH)_x/Ta_3N_5$ indeed suffer surface oxidation. It is because $Co(OH)_x$ and Co_3O_4 WOCs can greatly alleviate the unfavorable accumulation of photogenerated holes by accelerating the water oxidation kinetics with the assistance of NaOH. Unsatisfactory photostability performance is observed on Co_3O_4/Ta_3N_5 photoanode in 0.5 M Na_2SO_4 (pH = 6.5), and surprisingly much richer N content is detected compared to Co_3O_4/Ta_3N_5 measured in 1 M NaOH solution after photostability test (shown in Figure 7c). The larger peak area of N 1s might suggest the detachment even dissolution of Co_3O_4 from Ta_3N_5 surface and correspondingly enhanced exposure of Ta_3N_5 surface. Panel (d) in Figure 7 presents the Co 2p peaks of Co_3O_4/Ta_3N_5 photoanodes before and after the photostability test, and no perceivable differences were observed before photostability measurement. The decreased Co 2p peak area in Co_3O_4/Ta_3N_5

photoanode performed in 0.5 M Na_2SO_4 indicates the diminished Co_3O_4 coverage. It is reasonable to consider that in the case of Na_2SO_4 electrolyte O_2 production is accompanying with decreased pH value of neighbouring electrolyte, and instable nature of Co_3O_4 in acidic environment may initiate detachment even dissolution of Co_3O_4 from Ta_3N_5 surface.[18] As a result, it seems plausible that the diminished Co_3O_4 coverage is responsible for the unexpected increase in N 1s peak area for Co_3O_4/Ta_3N_5 tested in Na_2SO_4 electrolyte.

Effects of WOCs on the stability are usually evaluated by the oxidation degree of Ta_3N_5 surface.[15] Contrary to previous reports, we demonstrate that photostability is not always consistent with N content of Ta_3N_5 surface. Specifically, Co_3O_4/Ta_3N_5 photoanode possesses larger N content but exhibits extremely poor photostability when tested in Na_2SO_4 comparing with that tested in 1 M NaOH. The influence of WOCs on the N detection by XPS should be taken in consideration, for they conceal the Ta_3N_5 surface and they may peel off during PEC measurement, resulting in enhanced exposure of Ta_3N_5 surface. These extraordinary but rational N contents variation presented here demonstrates that probing N content is not a precise strategy for evaluating the photostability of Ta_3N_5 photoelectrode.

2.7. Photocurrent Action Spectra and Photoresponse of Co_3O_4/Ta_3N_5 Composite Photoanodes Under AM 1.5 G Illuminaion

To display a more acceptable and standard form of PEC performance on the Co_3O_4/Ta_3N_5 electrode, the incident photon to current efficiency (IPCE) was measured under monochromatic light irradiation and plotted as a function of wavelength at various voltages, the results of which are shown in **Figure 8**. With IPCE value of 26% at 400 nm and 24% at 550 nm under 1.2 V vs. RHE as well as 40% at 400 nm and 36% 550 nm under

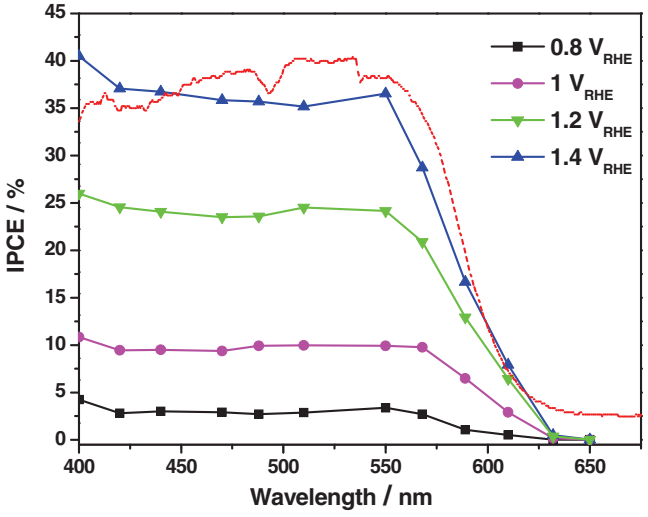

Figure 8. Incident photon to current efficiency (IPCE) spectra of the Co_3O_4/Ta_3N_5 electrode at 1.4 V vs. RHE (blue), 1.2 V vs. RHE (green), 1.0 V vs. RHE (mauve), 0.8 V vs. RHE (black). All the data were collected in 1 M NaOH solution. The absorption spectrum of bare Ta_3N_5 photoanode is also shown for reference (dotted red).

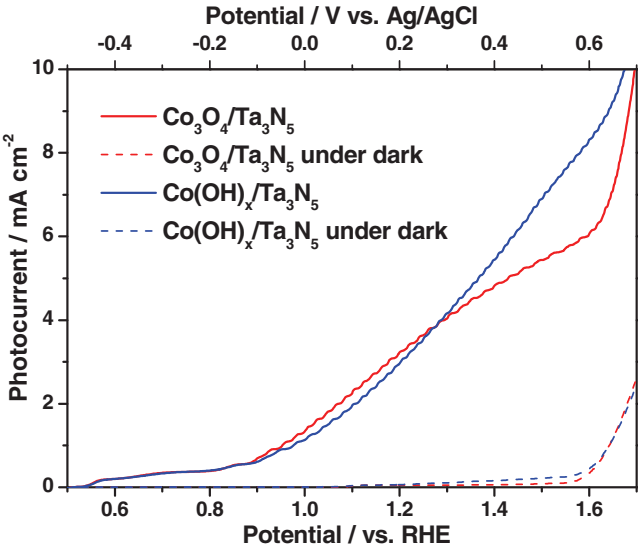

Figure 9. Current-voltage characteristics of Co_3O_4/Ta_3N_5 and $Co(OH)_x$/Ta_3N_5 photoanodes in the dark and under AM 1.5 G 100 mW/cm^2 simulated sunlight at a scan rate of 30 mV/s, measured in 1 M NaOH.

1.4 V vs. RHE, this photoelectrode has fairly exceeded previously reported bare Ta_3N_5 electrodes, including highly oriented Ta_3N_5 nanotube array photoanode.[16,26] IPCE values increase with increasing externally applied bias, on account of electrical bias facilitating the separation of the electron-hole pairs. Nearly 2.5-fold enhancement of IPCE from 10% to 25% in the visible light range of 400 to 550 nm is achieved when the applied bias is elevated from 1.0 to 1.2 V vs. RHE. However, under lower bias the IPCE value decreases steeply, and the PEC performance of Co_3O_4/Ta_3N_5 photoanode is far from satisfactory, which may root from the intrinsically high defective feature of Ta_3N_5 material. Efforts to increase the IPCE values under lower bias are still underway in our laboratory. Furthermore, the photocurrent response of Co_3O_4/Ta_3N_5 film exhibits almost the same feature as the absorption spectrum of Ta_3N_5 electrode film, suggesting that the observed photocurrent is based on band gap transition of Ta_3N_5.

It is necessary to present more visual information on the PEC performance of Co_3O_4/Ta_3N_5 under standard condition. Then we conducted photocurrent-voltage measurement under AM 1.5 G 100 mW/cm^2 simulated sunlight condition. **Figure 9** represents the obtained current-voltage curve of Co_3O_4/Ta_3N_5 photoanode, and $Co(OH)_x$/Ta_3N_5 is also shown for comparison. The dark current of $Co(OH)_x$/Ta_3N_5 anode is slightly higher than Co_3O_4/Ta_3N_5 anode up to about 1.6 V vs. RHE, where the fierce electrocatalytic oxygen evolution starts and dark currents increase strongly. The photocurrent curve of Co_3O_4/Ta_3N_5 anode depicts an almost linear rise from 0.9 V to 1.4 V vs. RHE, after which the increase of photocurrent becomes slow, and finally the plateau photocurrent of about 6 mA/cm^2 appears at 1.6 V vs. RHE before the drastic climb of dark current. By contrast, the photocurrent curve of $Co(OH)_x$/Ta_3N_5 film experiences a much steeper rise between 1.0 V and 1.6 V vs. RHE and reaches the maximum photocurrent as high as 8 mA/cm^2 at 1.6 V vs. RHE. The full potential of Co_3O_4/Ta_3N_5 anode is

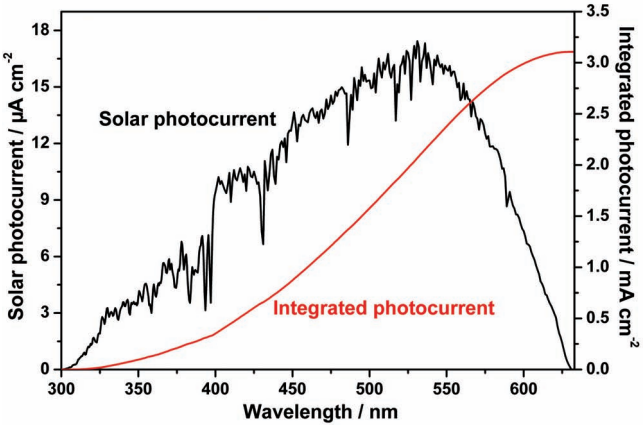

Figure 10. Solar photocurrent spectrum of the Co_3O_4/Ta_3N_5 electrode at 1.2 V vs. RHE obtained by multiplication of its IPCE spectrum with the photon flux spectrum of global sunlight (100 mW/cm^2 AM 1.5 G) (black). Integrated photocurrent under global sunlight between 300 nm and 630 nm (red).

much lower than that of $Co(OH)_x/Ta_3N_5$ film (6 mA/cm^2 versus 8 mA/cm^2), which can be attributed to the unfavorable oxidation of Ta_3N_5 during heat treatment on Co_3O_4/Ta_3N_5 anode. Despite of damaging heat treatment, photocurrent density as high as 3.18 mA/cm^2 is obtained on Co_3O_4/Ta_3N_5 electrode at 1.2 V vs. RHE, while 2.9 mA/cm^2 is achieved by $Co(OH)_x/Ta_3N_5$ film. The slightly larger photocurrent on Co_3O_4/Ta_3N_5 electrode may benefit from the contribution of high energy photons ($\lambda \leq$ 420 nm). Note that $Co(OH)_x$ loading greatly facilitates the performance at higher bias, while Co_3O_4/Ta_3N_5 electrode exhibits better performance at more cathodic potentials. This behavior of Co_3O_4/Ta_3N_5 photoanode again emphasizes the importance of abundant and compact interfaces, for these interfaces greatly facilitate efficient transfer of photogenerated holes at lower bias. Overall, the data collected under AM 1.5 G illumination demonstrate the great potential of Co_3O_4/Ta_3N_5 as high efficient photoelectrode, and there is much room for further improvement of Co_3O_4/Ta_3N_5 photoanode through more smart loading methods of Co_3O_4 WOC.

To verify the photocurrent value at 1.2 V vs. RHE, multiplication of the obtained IPCE spectrum with standard solar spectral distribution was carried out, yielding the solar photocurrent spectrum (see **Figure 10**). The total photocurrent obtained by integration over the solar photocurrent spectrum is 3.12 mA/cm^2 at 1.2 V vs. RHE, while the measured value is 3.18 mA/cm^2. The negligible difference between the calculated and tested photocurrent values states that the light source precisely simulated the AM 1.5 G solar emission in the photocurrent responsive range of Ta_3N_5 electrode, and the IPCE values as well as photocurrent under AM 1.5 G simulated sunlight are credible.

3. Conclusions

In summary, prominent improvement in photostability of Ta_3N_5 photoanode for PEC water splitting has been experimentally demonstrated. In detail, by employing robust and cheap Co_3O_4 nanoparticles WOC, about 75% of initial stable photocurrent maintains after 2 h irradiation at 1.2 V vs. RHE, which gives to date the best durability against photocorrosion by comparing with $Co(OH)_x/Ta_3N_5$ and IrO_2/Ta_3N_5 photoanodes under the same condition. On top of good photostability, Co_3O_4 nanoparticles loaded Ta_3N_5 photoanode achieves photocurrent density as high as 3.1 mA/cm^2 at 1.2 V vs. RHE with backside illumination under 1 sun AM 1.5 G simulated sunlight. The uniform distribution of Co_3O_4 nanoparticles WOC on Ta_3N_5 surface coupling with the abundant and compact nano-junctions formed between Co_3O_4 and Ta_3N_5 contribute to the relatively high stability. The poor proton-accepting property of Na_2SO_4 induced kinetic bottleneck of O_2 evolution is circumvented by replacing Na_2SO_4 with NaOH, and remarkably improved photocurrent stability is realized in the presence of both Co_3O_4 nanoparticles WOC and NaOH electrolyte. Our finding sheds light on the importance of accelerating the kinetics of water oxidation for the improvement of photostability on Ta_3N_5 photoelectrodes, and the kinetics of water oxidation is associated with both WOCs and the electrolytes. Only by parallel optimization of both WOCs and the electrolytes can we achieve efficient and steady O_2 evolution. To make it more intriguing, the present simple loading strategy actually enables uniform distribution and compact nano-junctions of Co_3O_4 WOC on Ta_3N_5 photoanode surface and opens a broad prospect for the practical application of these (oxy)nitrides photoelectrodes. Further improvement of the performance of these Ta_3N_5 photoanodes will be focused on enhancing IPCE values at lower voltages, by choosing efficient loading method as well as optimizing processing temperature and WOCs loading amounts of Co_3O_4 nanoparticles WOCs. These investigations are now ongoing in our lab, and we believe other (oxy)nitrides photoelectrodes, examples including $SrNbO_2N$, TaON, $LaTiO_2N$ and $LaTaON_2$, can also be stabilized through this unique strategy.

4. Experimental Section

Fabrication of Ta_3N_5 Photoanode: In the light of recent report on TaON and Ta_3N_5 photoanodes fabricated using electrophoresis deposition (EPD) method followed by necking treatment, we prepared Ta_3N_5 photoelectrode in a similar way.[15,22] Ta_3N_5 powder was synthesized by heating Ta_2O_5 powder at 1123 K for 15 h under a flow of ammonia gas (flow rate: 500 mL/min). Ta_3N_5 powder suspension for EPD was obtained by dispersing iodine (10 mg) and Ta_3N_5 (40 mg) powder in acetone (50 mL) with the assistance of sonication. EPD process was conducted between two parallel FTO electrodes with the distance of 1 cm under 10 V of bias for 3 minutes. The area of Ta_3N_5 film was ca. 1 cm × 1 cm, the amount of Ta_3N_5 powder deposited on FTO electrode was ca. 0.35 mg. The electrode was dried in air, and then dropped with $TaCl_5$ methanol solution (10 mM, 10 μL). This procedure was repeated for five times. Finally, the dropped electrode was then heated at 773 K for 30 minutes (NH_3 flow rate: 500 mL/min).

Deposition of Co Species WOCs on Ta_3N_5 Photoanode: The deposition of Co species WOCs onto Ta_3N_5 photoanode was carried out by an impregnation method as the following procedures. The colloidal $Co(OH)_x$ solution was firstly prepared by the addition of NaOH into an aqueous solution containing Co^{2+} ions. The Ta_3N_5 electrode was then immersed into the as prepared $Co(OH)_x$ colloidal solution for 1 h, washed with distilled water and then dried in air. The amount of $Co(OH)_x$ loaded onto Ta_3N_5 electrode was determined by energy dispersive X-ray (EDX) analysis. When it came to Co_3O_4 loading, $Co(OH)_x/Ta_3N_5$ electrode was calcined at 573 K for 10 minutes in air.

Photoelectrochemical Characterization: Photoelectrochemical measurements were carried out in a three-electrode configuration using an aqueous hydroxide electrolyte (1 M NaOH, pH 13.6), with Ta_3N_5 film as the working electrode, Ag/AgCl as the reference electrode, and Pt foil as the counter electrode. Potentials are reported vs. reversible hydrogen electrode (RHE), which is obtained using the formula $E_{RHE} = E_{Ag/AgCl} + 0.0591pH + 0.1976$ V. Photocurrent densities under visible-light irradiation were obtained by using a 500 W xenon lamp fitted with a cut-off filter (Hoya L-42). All films were illuminated from the backside of the Ta_3N_5 photoanodes. The irradiated area was circular with a diameter of ca. 6 mm and photocurrent densities were normalized to 1 cm^2. The incident photon to current efficiency (IPCE) was measured under monochromatic light irradiation, provided by the xenon lamp equipped with band pass filters. The light intensity was obtained with a photometer (Newport, 840-C).

Sample Characterization: The crystal structures of all the samples were measured by powder x-ray diffraction (XRD, Rigaku Ultima III) with Cu Kα radiation (λ = 1.54056 Å). The optical absorption spectra of the samples were performed on an UV-visible (UV-VIS) spectrophotometer (Shimadzu, UV-Vis 2550). The morphology of the Ta_3N_5 photoanodes was observed by field-emission scanning electron microscopy (FE-SEM; Nova NanoSEM 230, FEI) and EDX analyses were performed by an adjunct energy dispersive spectrometer. No conductive coating was deposited onto samples for these measurements. TEM analysis was conducted on a high-resolution transmission electron microscope (JEM-2100). The surface nitrogen contents were analyzed using X-ray photoelectron spectroscopy (XPS; Thermo Scientific K-Alpha).

Supporting Information

Supporting Information is available from the Wiley Online Library or from the author.

Acknowledgements

M.J.L. and F.Y.F. contributed equally to this work. This work is supported by a Project Funded by the Priority Academic Program Development of Jiangsu Higher Education Institutions, the National Natural Science Foundation of China (Nos. 21073090, 11174129 and 50902068), the National Basic Research Program of China (Grants No. 2011CB933303), the Jiangsu Provincial Science and Technology Research Program (Grant No. BK2011056). This article was amended on July 24, 2012. The greyscale figures that were originally published online were replaced with color versions.

Received: December 7, 2011
Revised: February 9, 2012
Published online: April 17, 2012

[1] a) A. Heller, *Science* **1984**, *223*, 1141; b) M. Grätzel, *Nature* **2001**, *414*, 338; c) N. S. Lewis, D. G. Nocera, *Proc. Natl. Acad. Sci. USA* **2006**, *103*, 15729; d) N. S. Lewis, *Science* **2007**, *315*, 798; e) C. Grimes, O. K. Varghese, S. Ranjan, *Light, Water, Hydrogen*, Springer, New York **2007**.
[2] A. Fujishima, K. Honda, *Nature* **1972**, *238*, 37.
[3] a) D. K. Zhong, M. Cornuz, K. Sivula, M. Gräetzel, D. R. Gamelin, *Energy Environ. Sci.* **2011**, *4*, 1759; b) M. Zhang, W. Luo, Z. Li, T. Yu, Z. Zou, *Appl. Phys. Lett.* **2010**, *97*, 042105; c) D. K. Zhong, D. R. Gamelin, *J. Am. Chem. Soc.* **2010**, *132*, 4202; d) S. D. Tilley, M. Cornuz, K. Sivula, M. Gräetzel, *Angew. Chem. Int. Ed.* **2010**, *49*, 6405; e) D. K. Zhong, J. Sun, H. Inumaru, D. R. Gamelin, *J. Am. Chem. Soc.* **2009**, *131*, 6086; f) A. Kay, I. Cesar, M. Gräetzel, *J. Am. Chem. Soc.* **2006**, *128*, 15714; g) I. Cesar, A. Kay, J. Martinez, M. Grätzel, *J. Am. Chem. Soc.* **2006**, *128*, 4582.
[4] a) B. D. Alexander, P. J. Kulesza, L. Rutkowska, R. Solarska, J. Augustynski, *J. Mater. Chem.* **2008**, *18*, 2298–2303; b) C. Santato, M. Odziemkowski, M. Ulmann, J. Augustynski, *J. Am. Chem. Soc.* **2001**, *123*, 10639; c) C. Santato, M. Ulmann, J. Augustynski, *J. Phys. Chem. B* **2001**, *105*, 936.
[5] a) M. Long, W. Cai, H. Kisch, *J. Phys. Chem. C* **2008**, *112*, 548; b) K. Sayama, A. Nomura, T. Arai, T. Sugita, R. Abe, M. Yanagida, T. Oi, Y. Iwasaki, Y. Abe, H. Sugihara, *J. Phys. Chem. B* **2006**, *110*, 11352; c) K. Sayama, A. Nomura, Z. G. Zou, R. Abe, Y. Abe, H. Arakawa, *Chem. Commun.* **2003**, 2908; d) W. Luo, Z. Yang, Z. Li, J. Zhang, J. Liu, Z. Zhao, Z. Wang, S. Yan, T. Yu, Z. Zou, *Energy Environ. Sci.* **2011**, *4*, 4046; e) H. Ye, H. S. Park, A. J. Bard, *J. Phys. Chem. C* **2011**, *115*, 12464.
[6] E. R. Young, R. Costi, S. Paydavosi, D. G. Nocera, V. Bulovic, *Energy Environ. Sci.* **2011**, *4*, 2058.
[7] J. J. H. Pijpers, M. T. Winkler, Y. Surendranath, T. Buonassisi, D. G. Nocera, *Proc. Natl. Acad. Sci. USA* **2011**, *108*, 10056.
[8] Y. W. Chen, J. D. Prange, S. Duehnen, Y. Park, M. Gunji, C. E. D. Chidsey, P. C. McIntyre, *Nat. Mater.* **2011**, *10*, 539.
[9] O. Khaselev, J. A. Turner, *Science* **1998**, *280*, 425.
[10] T. Takata, G. Hitoki, J. N. Kondo, M. Hara, H. Kobayashi, K. Domen, *Res. Chem. Intermed.* **2007**, *33*, 13.
[11] M. Hara, G. Hitoki, T. Takata, J. N. Kondo, H. Kobayashi, K. Domen, *Catal. Today* **2003**, *78*, 555.
[12] A. Kasahara, K. Nukumizu, T. Takata, J. N. Kondo, M. Hara, H. Kobayashi, K. Domen, *J. Phys. Chem. B* **2003**, *107*, 791.
[13] W. J. Chun, A. Ishikawa, H. Fujisawa, T. Takata, J. N. Kondo, M. Hara, M. Kawai, Y. Matsumoto, K. Domen, *J. Phys. Chem. B* **2003**, *107*, 1798.
[14] a) A. B. Murphy, P. R. F. Barnes, L. K. Randeniya, I. C. Plumb, I. E. Grey, M. D. Horne, J. A. Glasscock, *Int. J. Hydrogen Energy* **2006**, *31*, 1999; b) D. Yokoyama, H. Hashiguchi, K. Maeda, T. Minegishi, T. Takata, R. Abe, J. Kubota, K. Domen, *Thin Solid Films* **2011**, *519*, 2087.
[15] M. Higashi, R. Abe, K. Domen, *Energy Environ. Sci.* **2011**, *4*, 4138.
[16] A. Ishikawa, T. Takata, J. N. Kondo, M. Hara, K. Domen, *J. Phys. Chem. B* **2004**, *108*, 11049.
[17] W. Luo, B. Liu, Z. Li, Z. Xie, D. Chen, Z. Zou, R. Zhang, *Appl. Phys. Lett.* **2008**, *92*, 262110.
[18] M. Hamdani, R. N. Singh, P. Chartier, *Int. J. Electrochem. Sci.* **2010**, *5*, 556.
[19] G. Spinolo, S. Ardizzone, S. Trasatti, *J. Electroanal. Chem.* **1997**, *423*, 49.
[20] A. J. Esswein, M. J. McMurdo, P. N. Ross, A. T. Bell, T. D. Tilley, *J. Phys. Chem. C* **2009**, *113*, 15068.
[21] V. G. Hadjiev, M. N. Iliev, I. V. Vergilov, *J. Phys. C: Solid State Phys.* **1988**, *21*, L199.
[22] R. Abe, M. Higashi, K. Domen, *J. Am. Chem. Soc.* **2010**, *132*, 11828.
[23] M. Hara, E. Chiba, A. Ishikawa, T. Takata, J. N. Kondo, K. Domen, *J. Phys. Chem. B* **2003**, *107*, 13441.
[24] R. Boggio, A. Carugati, S. Trasatti, *J. Appl. Electrochem.* **1987**, *17*, 828.
[25] Y. Surendranath, M. Dincă, D. G. Nocera, *J. Am. Chem. Soc.* **2009**, *131*, 2615.
[26] X. J. Feng, T. J. LaTempa, J. I. Basham, G. K. Mor, O. K. Varghese, C. A. Grimes, *Nano Lett.* **2010**, *10*, 948.